

Two-dimensional laser-induced fluorescence imaging of metastable density in low-pressure radio frequency argon plasmas with added O₂, Cl₂, and CF₄

Brian K. McMillin^{a)} and M. R. Zachariah

Chemical Science and Technology Laboratory, National Institute of Standards and Technology, Gaithersburg, Maryland 20899

(Received 14 June 1995; accepted for publication 22 September 1995)

The effect of minor additions of O₂, Cl₂, and CF₄ on the argon metastable relative density and spatial distribution in low-pressure, radio-frequency argon plasmas, generated within a parallel-plate Gaseous Electronics Conference reference reactor, has been investigated using planar laser-induced fluorescence imaging. For the conditions examined (33.3 Pa, 75–300 V, <10 W), the addition of only a few percent of these electron attaching gases was found to decrease the metastable density by as much as an order of magnitude, despite the fact that the excited-state argon emission indicated an increase in the metastable production rate. In the dilute O₂/Ar discharges examined here, the spatial distribution of metastables was similar to that of the electropositive, pure argon cases, exhibiting a strong axial peak near the interface between the plasma bulk and the sheath at the powered electrode. In contrast, the addition of either Cl₂ or CF₄ was found to significantly modify the spatial distribution of the emission intensity and metastable density, resulting in a more symmetric and uniform axial metastable distribution. This change in metastable distribution for these mixtures was particularly apparent at lower powers and/or higher Cl₂/CF₄ concentrations, and suggests a transition from an electropositive to a somewhat electronegative discharge.

[S0021-8979(96)08401-4]

I. INTRODUCTION

Low-pressure radio-frequency (rf) plasmas are used extensively in the deposition and etching of thin films during microelectronics device manufacturing. Consequently, in recent years there has been a considerable effort aimed at developing models to improve the understanding, performance, and control of these processing plasmas.¹ One of the impediments to model development, though, has been the general lack of experimental data needed for input to these models. As Graves² has recently noted, there is a significant need for fundamental cross section and rate coefficient data for the chemical species relevant to low-pressure, low-temperature reactive plasma processing. Similarly, there is also a need for plasma property measurements (e.g., species concentration) for the verification of these models.

To address the latter, we recently reported³ two-dimensional (2D) measurements of the argon metastable density field as a function of pressure and applied voltage in pure argon rf discharges. Those measurements are of interest because (1) argon plasmas are simple enough and have a sufficiently well-developed database to be amenable to multidimensional modeling and (2) they are one of the first complete 2D maps of species concentration of any kind in a low-pressure rf plasma. Here we extend those 2D measurements of metastable density to argon plasmas diluted with a small percentage of an attaching gas, namely O₂, CF₄, or Cl₂.

The purpose of this study is to investigate what effect the added attaching gas has upon the discharge structure by mapping the spatial distribution of argon metastable density with planar laser-induced fluorescence (PLIF) imaging. Our motivation for this work results from the fact that, while the addition of even small amounts of an electronegative gas to an argon discharge is known to significantly quench the metastable density^{4–8} and to make the discharge electronegative in nature,^{9,10} the experimental data currently available for even these simple mixtures are limited. Further, these expected changes in the metastable density distribution, combined with the fact that these measurements were obtained from a well-characterized reactor (the Gaseous Electronics Conference or GEC reference cell),¹¹ make the present results useful for validation of plasma models. Indeed, these particular attaching gases were chosen because of their relatively well-known cross sections and rate coefficients (see, e.g., Refs. 12–14) as well as their importance for plasma etching applications.¹⁵

In the following sections, we briefly describe the experimental setup and then discuss results of metastable measurements in dilute (<5%) O₂/Ar, CF₄/Ar, and Cl₂/Ar mixtures. In addition, excited-state optical emission measurements of the glow region, and voltage and current data measured at the powered electrode are presented and used to help interpret changes in the metastable density field. The results discussed here were all obtained at 33.3 Pa (250 mTorr), applied voltages of 75–300 V, and powers of less than 10 W.

II. EXPERIMENTAL DETAILS

The GEC reference cell,¹¹ the rf electrical diagnostics,^{16,17} and the PLIF imaging system³ used in these

^{a)}National Research Council NIST postdoctoral research associate, 1993–1995; Current address: Lam Research Corp., 4650 Cushing Parkway, Fremont, CA 94538; Electronic mail: brian.mcmillin@lamrc.com

experiments have been described previously, but for completeness, we will briefly review the salient details. The stainless steel cell is configured as a capacitively coupled, parallel-plate reactor with 10.2-cm-diam aluminum electrodes and a 2.25 cm interelectrode spacing. The lower electrode is powered by a 13.56 MHz rf power supply and matching network, coupled through a rf isolating filter. The upper electrode and the remainder of the chamber is grounded. Voltage and current wave forms are measured with probes located at the base of the powered electrode (after the matching network) and acquired with a digitizing oscilloscope. An additional probe is used to measure the current wave form at the ground electrode. From these two current measurements we can determine what fraction of input current flows to the ground electrode and what fraction flows radially out of the plasma to the chamber walls.¹⁷ To determine the actual voltage, current, and power supplied to the plasma, these measured wave forms were Fourier analyzed and corrected for cell parasitics.^{16,17} The applied voltages referred to below correspond to the peak-to-peak amplitudes of the measured (uncorrected) voltage wave forms.

The feed gas mixture (made with Ar 99.999%, Cl₂ 99.99%, CF₄ 99.9%, O₂ 99.98% purity gases) was delivered to the chamber through mass flow controllers at a flow rate of 25 sccm, and introduced through a showerhead arrangement of holes in the upper electrode. The cell pressure was maintained at 33.3 Pa (250 mTorr) using a mechanical vacuum pump in conjunction with a feedback-controlled exhaust throttling valve. The cell pressure was monitored using a capacitance manometer, which provided the input signal to the throttle-valve controller. Prior to each set of experiments, the cell was typically evacuated to a base pressure of 1×10^{-5} Pa (1×10^{-7} Torr) using a turbomolecular pump.

The metastable density fields were measured using PLIF imaging; for more details on the PLIF technique, the reader is referred to Refs. 15 and 18 regarding its application to glow discharges, and to Ref. 19 regarding general information. In particular, the argon $1s_5$ metastable density was measured by exciting the $1s_5 \rightarrow 3p_2$ transition near 395 nm and detecting the resulting fluorescence at ~ 418 and ~ 433 nm (i.e., the $3p_2 \rightarrow 1s_3$ and $3p_2 \rightarrow 1s_2$ transitions, respectively). A schematic diagram of the imaged region of the discharge is shown in Fig. 1. As indicated in Fig. 1, a thin laser beam (expanded and apertured to 2 mm thick by 25 mm tall) from a Nd:YAG pumped dye laser (10 ns pulse width, 3 mJ pulse energy, $\sim 1 \text{ cm}^{-1}$ linewidth) was directed into the reactor to excite fluorescence from the central vertical plane of the discharge. The fluorescence from the right-half of this illuminated plane was then imaged through an $f/4.5$ camera lens onto an intensifier-gated, cooled charge-coupled device (CCD) camera. Plasma emission images were also obtained with this camera by exposing the detector with no laser excitation.

The laser sheet entering the reactor was expanded to produce a fairly uniform energy distribution and was attenuated to a fluence of less than $\sim 0.1 \text{ mJ/cm}^2$ to reduce measurement uncertainties due to fluorescence saturation. To normalize the PLIF images for fluctuations in the laser energy and distribution, the laser sheet was monitored during

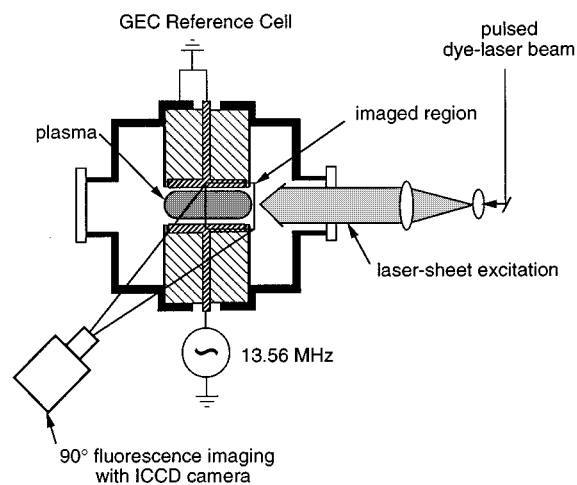


FIG. 1. Schematic of the imaged region of the discharge.

the experiments by directing a 5% reflection of the sheet onto a static dye cell and recording the resulting fluorescence with a video CCD camera and framegrabber computer board. These laser sheet normalizations were applied to the final PLIF images by software remapping the dye cell images from the video CCD to the intensified CCD coordinates, based on registration images obtained with the laser sheet masked.

While imaging the plasma, a combination of 410 nm long-pass and 450 nm short-pass filters was used to reject laser scattering and reduce the plasma emission reaching the intensified camera. This commercially available filter combination was chosen because its transmission function provided a good ratio of laser-induced fluorescence to plasma emission signal, i.e., signal-to-noise ratio, while efficiently rejecting laser scattering. (The raw PLIF images include an emission background which is subtracted during data reduction.) The PLIF images were acquired by time averaging the signal from 1000 laser shots, with the intensifier gate width set to ~ 500 ns to temporally integrate the entire fluorescence decay, while suppressing excessive plasma emission (to improve the signal-to-noise ratio). A synchronization pulse generated by the laser just prior to the laser firing served as the trigger to activate the intensifier for all image acquisitions. Time-averaged plasma emission images (an average of 1000 intensifier exposures triggered at 10 Hz with the laser blocked) were acquired in the same fashion, immediately following the completion of each (time-averaged) PLIF image acquisition. Since 1000 images were averaged for each case and the individual image acquisitions were not phase locked to the rf power supply, both the final PLIF and excited-state emission images should therefore represent true time averages. In all cases, the images were spatially averaged 2×2 pixels to improve the signal-to-noise ratio, resulting in an axial and radial resolution of $\sim 200 \mu\text{m}$.

To relate the signal in the raw fluorescence images to the metastable relative density, the plasma emission and the camera's dark background were first subtracted and then the images were corrected for fluorescence quenching and for spatial variations in the laser energy and detector response.³

As discussed previously,³ we applied a spatially uniform fluorescence yield correction, which is valid assuming that neutral argon dominates the fluorescence quenching. Neglecting the fluorescence quenching by the molecular diluents (and resulting radicals) is reasonable here because neutral argon has a relatively strong fluorescence quenching rate and accounts for $\sim 95\%$ of the composition of the plasma. In addition, the next most significant species (the undissociated molecular diluent) is expected to be (nearly) uniformly distributed throughout the discharge.

III. RESULTS

A. Metastable density measurements

Relative 2D measurements of the argon $1s_5$ metastables were obtained in pure argon and in argon plasmas diluted with ($<5\%$) of O_2 , CF_4 , or Cl_2 , to determine the effect of electron attaching gases on the metastable density and distribution. Metastable distributions were also measured as a function of applied voltage in pure argon, 0.4% Cl_2/Ar , and 0.8% CF_4/Ar mixtures to examine structural changes with varying degrees of molecular dissociation. All of these measurements were obtained at 33.3 Pa (250 mTorr) and at a flow rate of 25 sccm. The absolute metastable density was not determined in these experiments, but previous measurements in a pure argon discharge at similar conditions⁸ have indicated that the argon $1s_5$ metastable density is of the order of 10^{11} cm^{-3} . The estimated uncertainty in the relative number of densities within a given data set is $10\% - 15\%$, based largely on the reproducibility of the measurements. Slight differences in the fluorescence quenching for the various mixtures and in the laser energy/fluorescence saturation from day to day also contribute to the estimated uncertainty.

Figure 2 shows a series of contour plots of the metastable density distribution for pure argon and various O_2/Ar and CF_4/Ar discharges at a 200 V applied rf voltage. In Fig. 2 the $z=0$ and $z=2.25$ cm axial locations correspond to the powered and grounded electrodes, respectively. In all cases the metastable density shows fairly significant variations both axially and radially. Because of the asymmetric configuration of the reactor, the metastable density peaks (axially) near the powered electrode, i.e., a higher voltage drop (and, hence, electric field) across the powered sheath¹² leads to increased electron impact excitation there. Similarly, the metastables peak (radially) near the edge of the powered electrode, where previous measurements²⁰ have indicated an enhanced electric field.

Figures 2 and 3 show the addition of a molecular diluent results in a significant decrease of the metastable density, as expected.^{4,6,7} The addition of 2% oxygen [Fig. 3(a)], for example, results in about an order of magnitude decrease in the metastable density, but the metastable spatial distribution for these dilute O_2/Ar mixtures remains essentially the same as that of pure argon. On the other hand, the metastable quenching resulting from adding CF_4 is less significant than for O_2 , but the spatial distribution of the metastables with added CF_4 is, in some cases, substantially different from the pure argon and O_2/Ar cases. In particular, as the added CF_4 concentration is increased, the peak in the metastable density near the

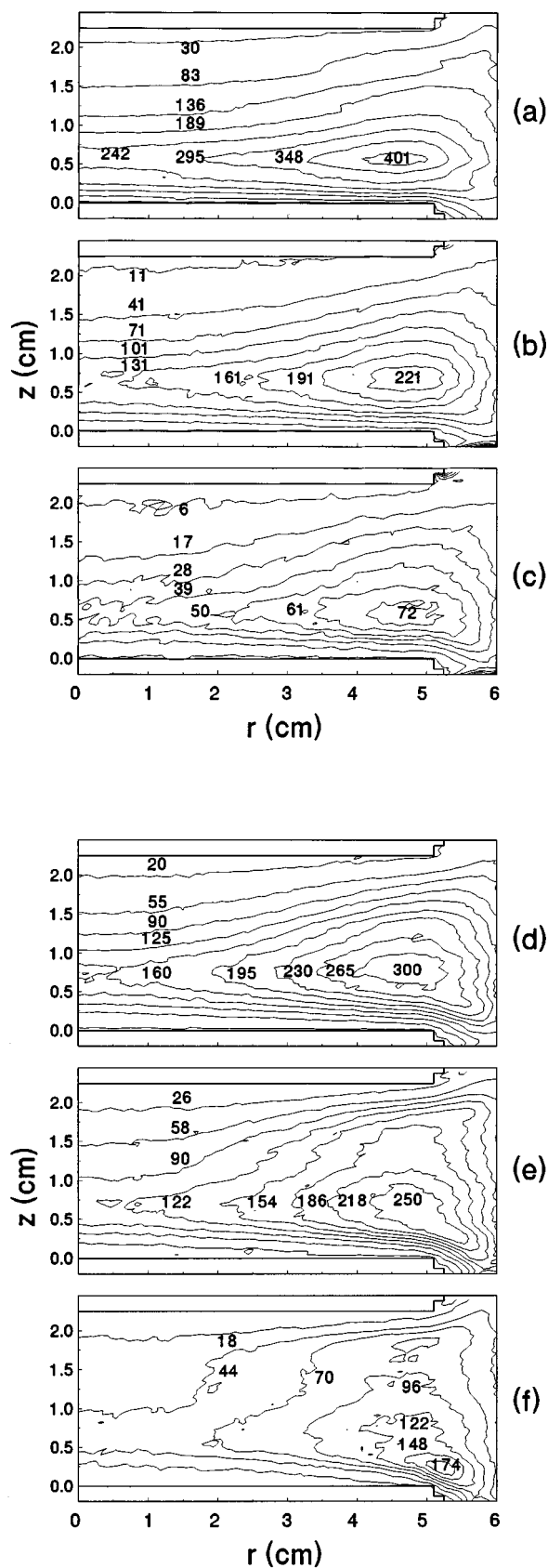


FIG. 2. Contour plots of the argon $1s_5$ relative density distribution at 33.3 Pa and an applied rf voltage of 200 V in argon plasmas with (a) no molecular additive, (b) 0.4% added O_2 , (c) 1.2% added O_2 , (d) 0.4% added CF_4 , (e) 1.2% added CF_4 , and (f) 3.6% added CF_4 . In the plots, $z=0$ and $z=2.25$ cm correspond to the powered and grounded electrodes, respectively.

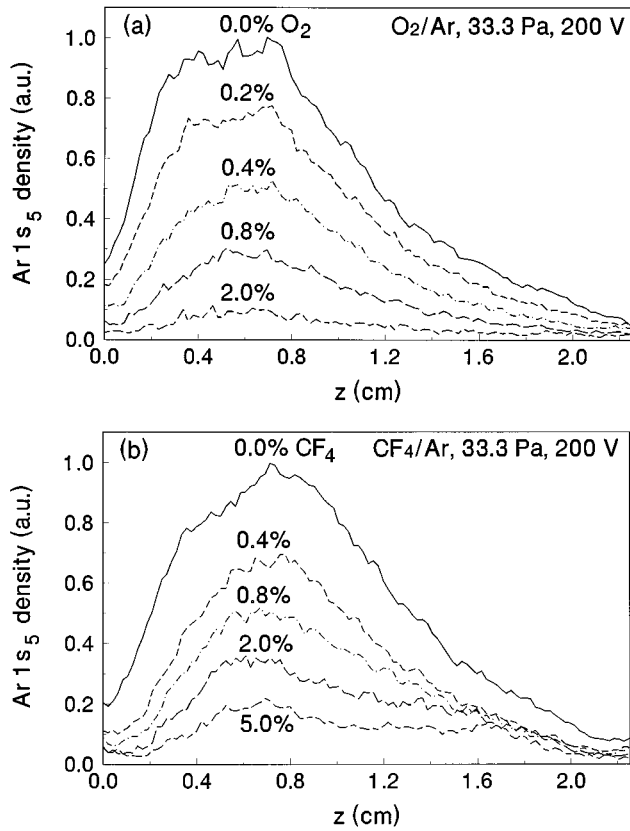


FIG. 3. Axial centerline ($r=0$) profiles of the argon $1s_5$ metastable density taken from the images of (a) O_2/Ar and (b) CF_4/Ar discharges in Fig. 2. The powered electrode is located at $z=0$ cm.

powered sheath/bulk interface becomes less pronounced, and a peak near the ground sheath/bulk interface appears, resulting in a somewhat more symmetric and uniform axial profile. These changes in metastable distribution may be seen more clearly in Fig. 3, which shows the centerline ($r=0$) axial metastable density profiles for the O_2/Ar and CF_4/Ar mixtures examined here. Although not shown, the Cl_2/Ar mixtures exhibited somewhat more significant quenching than the O_2/Ar mixtures, and a transition (similar to CF_4/Ar) to a more uniform metastable distribution with increasing concentration of Cl_2 .

The effect of varying the applied voltage on pure argon and 0.4% Cl_2/Ar discharges is shown in the series of contour plots of metastable density in Fig. 4. For the pure argon cases, as the applied voltage is increased the spatial distribution remains generally similar, but the metastable density increases and becomes more radially uniform. This increase in metastable density results from an increase in metastable production, as indicated by the increase in argon $5p \rightarrow 4s$ emission,³ and is consistent with an increase in power deposited in the plasma (see Table I). Similarly, the metastable density increases with applied voltage for the Cl_2/Ar discharges and, although not shown, for CF_4/Ar discharges as well. The increase in metastable density in these mixtures results, in part, from increased power deposition, but pre-

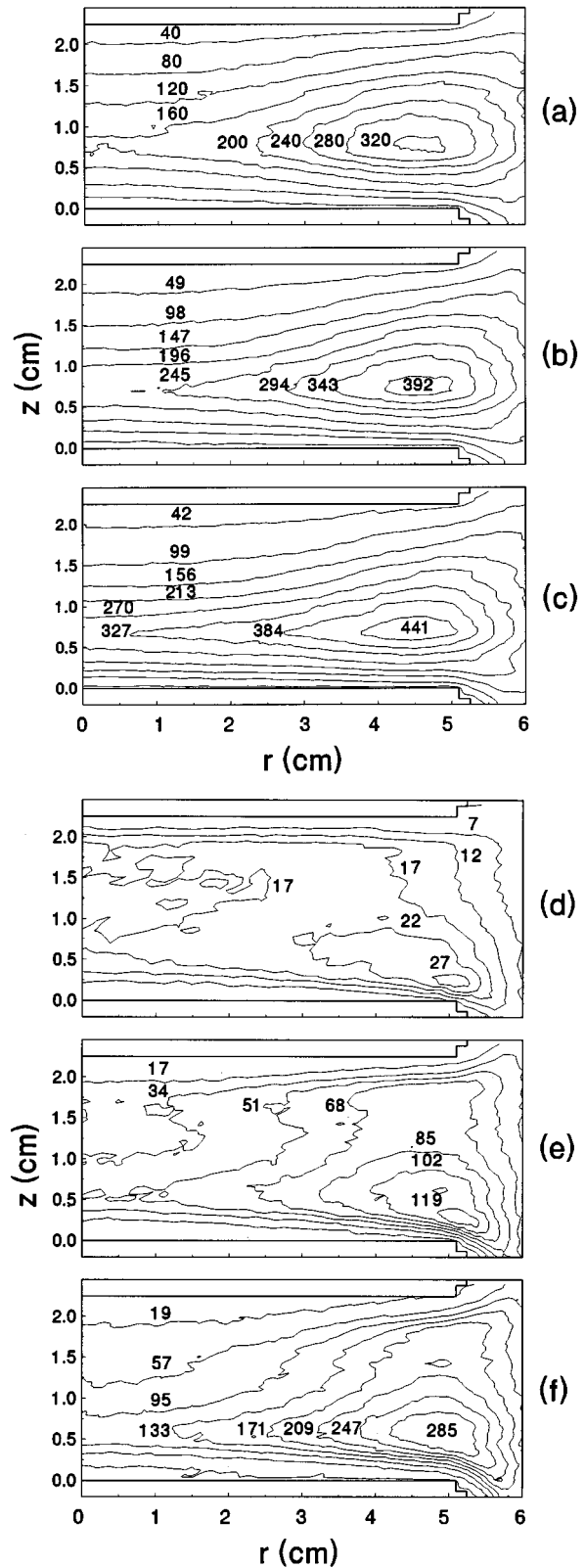


FIG. 4. Contour plots of the argon $1s_5$ relative density distribution in 33.3 Pa discharges as a function of applied voltage, for pure argon at (a) 75 V, (b) 150 V, and (c) 300 V; and for 0.4% Cl_2/Ar at (d) 75 V, (e) 150 V, and (f) 300 V, respectively. In the plots, $z=0$ and $z=2.25$ cm correspond to the powered and grounded electrodes, respectively.

sumably also from increased dissociation of the molecular additive which reduces the metastable quenching. In the Cl_2/Ar mixtures, for example, the atomic chlorine is expected to quench metastables less effectively than Cl_2 , be-

TABLE I. Amplitudes of the as-measured peak-to-peak voltage (V_{rf}), the magnitude (half of peak-to-peak) of the fundamental components of voltage (V_{pe}) and current (I_{pe}) at the powered electrode, the phase difference (ϕ) between the voltage and current at the powered electrode, the dc self-bias potential (V_{dc}), and the power at 33.3 Pa (250 mTorr).

Discharge	V_{rf} (V)	V_{pe} (V)	I_{pe} (mA)	ϕ (deg)	V_{dc} (V)	Power (W)	
Ar ^a	75	41	88	-68.3	-15.0	0.65	
	150	84	209	-76.4	-51.6	2.00	
	200	111	269	-78.4	-75.5	3.00	
	300	168	398	-80.0	-129	5.82	
0.2% O ₂ /Ar ^b	200	112	336	-77.6	-76.5	4.05	
	0.4%	200	111	324	-76.4	-69.9	4.23
	0.8%	200	111	309	-75.1	-66.4	4.38
	1.2%	200	112	303	-74.3	-67.8	4.61
	2.0%	200	110	279	-72.8	-64.9	4.53
0.2% Cl ₂ /Ar ^a	200	110	261	-70.5	-72.2	4.78	
	0.4%	200	110	250	-69.2	-69.0	4.89
	0.8%	200	109	244	-67.3	-63.2	5.18
	1.2%	200	110	242	-66.5	-60.1	5.28
	1.6%	200	110	238	-66.3	-59.1	5.32
0.4% CF ₄ /Ar ^a	200	110	236	-73.2	-63.9	3.75	
	0.8%	200	109	218	-70.2	-63.3	4.01
	2.0%	200	108	195	-66.3	-47.4	4.26
	3.6%	200	109	188	-66.1	-43.6	4.13
	5.0%	200	107	186	-65.2	-41.1	4.21
0.4% Cl ₂ /Ar ^a	75	41	61	-55.4	-14.4	0.72	
	0.4%	150	82	178	-65.7	-43.8	2.99
	0.4%	300	167	383	-73.7	-122	8.93
0.8% CF ₄ /Ar ^a	75	40	50	-57.2	-14.0	0.55	
	0.8%	150	81	143	-65.8	-37.2	2.39
	0.8%	300	165	333	-72.4	-109	8.30

^aSeasoned cell.

^bClean cell.

cause fewer Cl energy levels (relative to Cl₂) are available to absorb the energy transfer.⁷

In contrast to the pure argon cases, the spatial distribution of metastables in the Cl₂/Ar (and CF₄/Ar) discharges changes significantly with applied voltage. In particular, at the lower voltages in the Cl₂/Ar discharges (and CF₄/Ar), the axial metastable distribution is relatively symmetric and uniform. As the voltage is increased, however, the axial distribution becomes increasingly peaked near the powered sheath/plasma bulk interface. In addition, the fractional increase in the peak metastable density is larger for the argon/molecular mixtures than for the pure argon discharges. These trends can be seen more clearly in Fig. 5, which shows the centerline ($r=0$) axial metastable profiles at three voltages for the pure argon, 0.4% Cl₂/Ar, and 0.8% CF₄/Ar discharges, respectively. No measurements were obtained as a function of applied voltage for O₂/Ar discharges.

B. Electrical measurements

Voltage and current wave forms were measured near the base of the powered electrode to characterize the discharge and permit comparisons to model calculations and other experimental studies. Typical measurements of the current and

power input to pure argon and CF₄/Ar plasmas are shown in Fig. 6. In general, for all of the mixtures examined, the current and power flowing to the plasma increase with the applied peak-to-peak voltage. For a given applied voltage, the addition of an attaching gas generally leads to a decrease in current and an increase in power. The increase in power results from a more resistive impedance. Interestingly, the power increases more with applied voltage (75–300 V) for the CF₄/Ar (and Cl₂/Ar) mixtures than for pure argon. Table I shows additional electrical measurement results from these experiments. As noted above, these data were determined from a Fourier analysis of the measured wave forms using an equivalent circuit model of the GEC cell and the external circuitry.^{16,17} Shown in Table I is a compilation of the fundamental components of the voltage and current wave forms and their relative phase, the magnitude of the dc self-bias, and the power dissipated in the plasma.

In these electrical measurements, note that we make a distinction between “clean” and “seasoned” cell data: the data labeled with “clean cell” refer to experiments conducted prior to running plasmas containing CF₄; and the data labeled with “seasoned cell” refer to experiments conducted after cell exposure to CF₄-containing plasmas. It is well

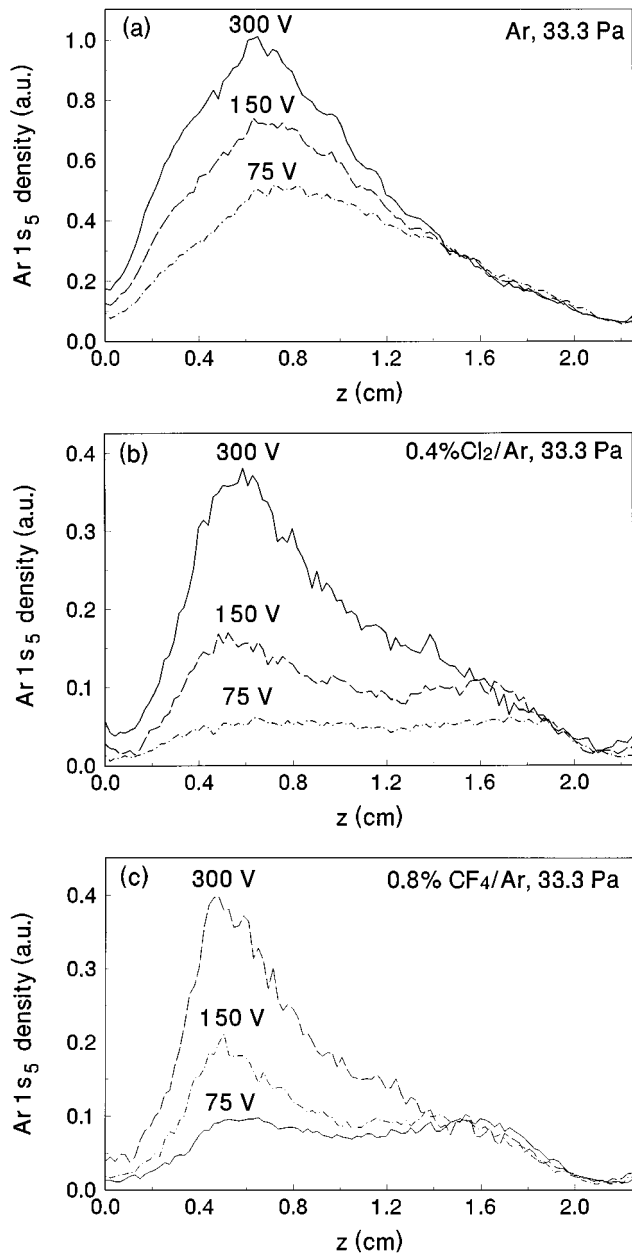


FIG. 5. Axial centerline ($r=0$) profiles of the argon metastable density taken from 2D laser-induced fluorescence images of 33.3 Pa discharges acquired as a function of applied voltage in (a) pure argon, (b) 0.4% Cl_2/Ar , and (c) 0.8% CF_4/Ar . The powered electrode is located at $z=0$ cm.

known that the electrical and chemical properties of the reactor can be modified by the deposition of fluorocarbon films on the inner wall and electrode surfaces (see, e.g., Ref. 21). With this in mind, prior to obtaining each seasoned cell data set, the reactor was cleaned with an oxygen plasma in an attempt to ensure a well-defined initial state for each experiment. Nevertheless, the baseline current and power characteristics for pure argon plasmas were noticeably and reproducibly lower ($\sim 10\%$ – 20% lower current) in the seasoned cell, even after a number of oxygen plasma cleans.

IV. DISCUSSION

A. Metastable formation and destruction

The local time-averaged argon metastable density results from a balance between metastable production and destruc-

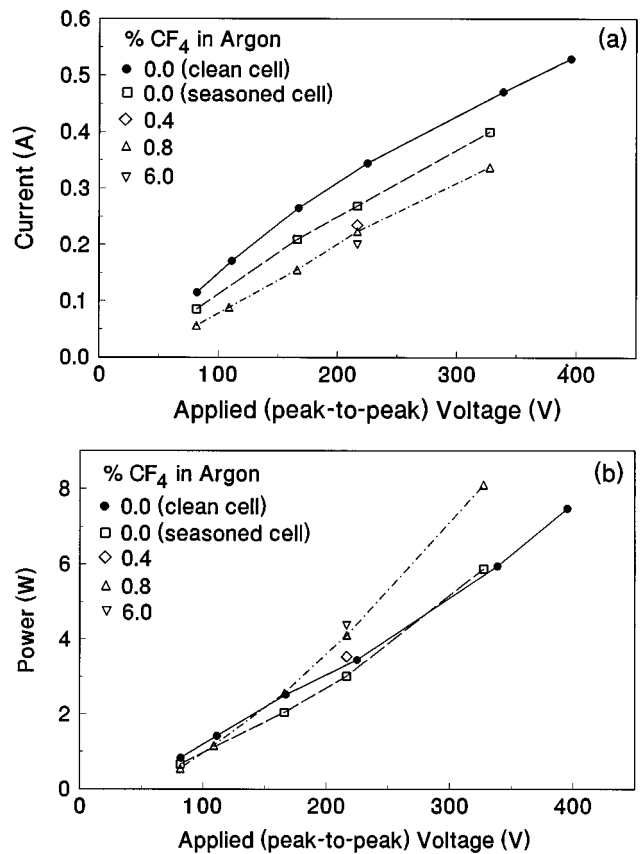


FIG. 6. Current (a) and power (b) at the fundamental frequency (13.56 MHz) vs corrected applied voltage for Ar and CF_4/Ar discharges.

tion processes. In these discharges, the metastables are primarily produced by direct electron-impact excitation, although cascading from more highly excited states can also contribute at some conditions.^{14,22} In the pure argon discharges considered here, the primary collisional loss mechanisms for the metastables are electron quenching (to nearby resonant and higher electronic states) and diffusion to the walls,^{7,23} while other loss mechanisms of lesser importance include stepwise ionization, metastable pooling, two- and three-body quenching, and superelastic electron quenching.²³ In argon/molecular discharges, however, molecular quenching can dominate the metastable destruction rate, even when the molecular additives are present in low concentrations. This can be inferred, at least qualitatively, by comparing the estimated metastable destruction rates for typical conditions of interest here, shown in Table II. It should be noted, though, that the actual quenching rates in the plasma will differ from these estimates because of molecular dissociation and a reduction of electron concentration (and, thus, electron quenching) due to attachment.

In general, a decrease in the metastable density can result from either a decrease in the production rate, an increase in the destruction rate, or a combination of both. In the present results, however, the decrease in the metastable density cannot be attributed to a decrease in production, because emission measurements, which (qualitatively) reflect the metastable excitation rate,³ show an increase in intensity with minor ($<5\%$) additions of these molecular additives

TABLE II. Estimated loss rates for argon metastables in discharges at 33.3 Pa (250 mTorr).

Mechanism	Rate expression ^a	Relative rate per unit metastable density ^b (s ⁻¹)	Ref.
Three-body quenching	$k_{3B} (N_{Ar})^2 N_{Ar_m}$	1	24
Two-body quenching	$k_{2B} N_{Ar} N_{Ar_m}$	3	24
Electronic quenching	$k_e N_e N_{Ar_m}$	30	24
Axial diffusion	$D_{Ar_m} N_{Ar_m} / \Lambda^2 P$	50	25
CF ₄ quenching	$k_{CF_4} N_{CF_4} N_{Ar_m}$	460	4
O ₂ quenching	$k_{O_2} N_{O_2} N_{Ar_m}$	2400	4
Cl ₂ quenching	$k_{Cl_2} N_{Cl_2} N_{Ar_m}$	5400	4

^a k is the appropriate rate coefficient, N is the number density for the species denoted by subscript, D_{Ar_m} is the metastable diffusion coefficient, $\Lambda \approx (\text{inter-electrode spacing})/\pi$ is the characteristic diffusion length, P is pressure, and the subscripts e , Ar , and Ar_m refer to the electrons, neutral argon, and metastable argon, respectively.

^bEstimated using the rate coefficients from the noted references and assuming $N_{Ar} = 8 \times 10^{15} \text{ cm}^{-3}$, $N_e = 10^9 \text{ cm}^{-3}$, and a 1% mole fraction of the respective molecular diluents.

(see Fig. 7). It should be emphasized that the increase in emission observed here is not likely to be due to a decrease in self-absorption (see Ref. 5 for a discussion of self-absorption), based on the results of absorption calculations for the $5p \rightarrow 4s$ transitions at our conditions.

This observed increase in emission (of $\leq 2\times$), and therefore in metastable production, with the addition of an attaching gas may seem counterintuitive, because the metastables are produced through electron impact collisions and the electron density decreases due to attachment. The metastable production rate, however, also depends on its rate coefficient as well as the electron and neutral argon densities. Consequently, the metastable production can increase here, as long as the increase in its rate coefficient is larger than the decrease in electron density through attachment. Indeed, recent modeling results¹⁴ have shown an increase in high energy excitation (and, hence, rate coefficient) in argon/attaching gas mixtures (compared to pure argon at similar conditions), because of an increase in the electric field to neutral density ratio (E/N) necessary to sustain the plasma. Hence, the in-

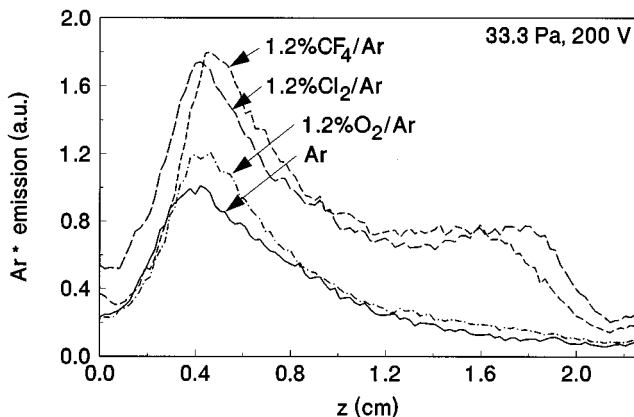
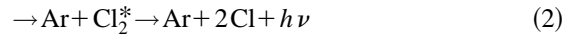
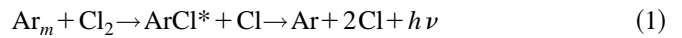


FIG. 7. Centerline ($r=0$) line-of-sight integrated $5p \rightarrow 4s$ argon emission profiles (410–450 nm) taken from the corresponding 2D images of plasma emission obtained for Ar, 1.2% O₂/Ar, 1.2% Cl₂/Ar, and 1.2% CF₄/Ar discharges at 200 V and 33.3 Pa. The powered electrode is located at $z=0$ cm.

crease in emission observed here may result, in part, from an increased rate coefficient for metastable production, associated with an increased E/N ratio in these argon/attaching gas discharges. In addition, the observed increase in emission (metastable production) may be due, in part, to an increased power deposition for these argon/molecular mixtures at constant applied voltage.

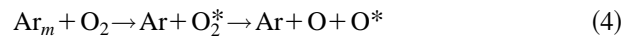
Because the increase in emission indicates an increase in metastable production, the decrease in metastable density observed in Fig. 3 can therefore only be attributed to a larger ($>2\times$) increase in the metastable destruction rate. Furthermore, since the electron density is expected to decrease with the addition of these attaching gases, we can assume that the decrease in metastable density is not due to an increase in electron quenching. In light of the estimated quenching rates in Table II, we therefore conclude that the decrease in metastable density results from an increase in quenching by the respective molecular additives and their dissociated fragments.

The reactions which lead to molecular quenching of argon metastables for the mixtures of interest here have been discussed previously.^{4–6} Of these, Cl₂ exhibits the highest metastable quenching rate with several possible pathways including:^{6,14}



where Ar_m indicates an argon metastable, $ArCl^*$ is an argon–chlorine excited state dimer, Cl_2^* is an electronically excited chlorine molecule, and $h\nu$ is the energy of an emitted photon.

Molecular oxygen also exhibits a moderately high quenching rate for argon metastables.⁴ This quenching by oxygen has previously been attributed to a near-resonant energy transfer between the metastable and a repulsive excited state of neutral O₂, leading to a dissociative transfer reaction.⁵ The ultimate products of this reaction are believed⁵ to be a neutral ground-state argon atom and two oxygen atoms:



where O_2^* is an excited, repulsive state of the oxygen molecule, and O is the ($2p^3P$) ground, O^* is the ($2p^1D_2$) excited, and O^{**} is the ($2p^1S_0$) excited state of atomic oxygen. CF₄, in contrast, exhibits a relatively low quenching rate for argon metastables,^{4,6} that presumably results in the dissociation of CF₄ by cleavage of the C–F bond. It has been argued⁶ that the relatively low quenching rate for CF₄ arises because the energy of its first excited state (>12 eV) is higher than that of the argon metastable (~ 11.5 eV). Hence, the metastable quenching by CF₄ is limited by a finite (albeit small) energy barrier.

At least qualitatively, the changes in the metastable density we observe are consistent with the quenching rates (and

mechanisms) summarized above, and with measurements reported by other investigators.^{7,24} With regard to additive concentration, for example, we found that the addition of Cl₂ produced the largest decrease in metastable density, followed by O₂, and CF₄, consistent with the estimates in Table II. We see no evidence, however, of an *initial increase* in metastable density at the plasma center previously observed for dilute attaching-gas/argon mixtures.⁷ We have no explanation for this, unless this discrepancy is due to the more symmetric nature of their discharge compared to ours.

B. Electron attachment and discharge electronegativity

The overall character of the low-pressure rf discharges of interest here depends to a large extent on their degree of electronegativity. In electropositive discharges (e.g., argon), the only charged particles present are electrons and positive ions. Electronegative discharges (e.g., Cl₂, CF₄, O₂), however, contain negative ions as well and, in strongly electronegative discharges, the negative ion density can be comparable to the positive ion density.¹² The formation of these negative ions can significantly reduce the electron density (by as much as one or more orders of magnitude) and change the electron energy distribution, thereby having a profound influence on the properties of the discharge. In electropositive discharges, for example, electrons are lost primarily through ambipolar diffusion; the electric field within the bulk is relatively small; the discharge impedance is essentially capacitive; and at the conditions of interest here, the ionization (and high energy excitation) primarily occurs near the powered sheath/bulk interface. On the other hand, in electronegative discharges, electrons are lost primarily through attachment; the lower electron density results in a more resistive (or, in some cases, inductive) discharge, with stronger bulk electric fields; and, generally, there is enhanced ionization (and high energy excitation) within the plasma bulk.^{25,26}

By adding even a few percent of an attaching gas to argon, one can change the nature of the discharge from electropositive to electronegative, as indicated by previous modeling results⁹ and experimental electrical and optical emission measurements.¹⁰ In the present Cl₂/Ar, CF₄/Ar, and, to a lesser extent, O₂/Ar discharges, we see evidence of a reduced electron number density, which is consistent with a transition from electropositive toward electronegative character. For example, although the effect is minor, the addition of O₂, CF₄, and Cl₂ is found to shift the phase of the plasma impedance toward 0°, which is indicative of a more resistive plasma bulk. For a given mixture fraction in Table I, the addition of Cl₂ shows the largest phase change, while O₂ shows the weakest, suggesting that Cl₂/Ar and O₂/Ar discharges are the most and least electronegative mixtures considered here, respectively. We have also observed that the fraction of input current which flows (axially) to the ground electrode, as opposed to flowing radially out to the chamber walls, increases with the concentration of attaching gas at 33.3 Pa and 200 V.²⁷ In addition, we have found that, for a given mixture (at 33.3 Pa), the fraction of current flowing to the ground electrode increases with decreasing applied voltage.²⁷ These relative increases in the current to the

ground electrode indicate a more confined discharge, and are consistent with a reduced electron density, resulting from attachment reactions (see below).

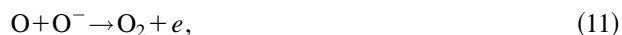
The change in the discharge character for these experiments is perhaps more evident in the optical measurements. As illustrated in Figs. 2–5, besides reducing the metastable density, the addition of an attaching gas to an argon discharge can alter the metastable spatial distribution as well, especially at lower powers and/or higher attaching gas concentrations. (For a given mixture, a lower power will result in less dissociation, which effectively increases the attaching gas concentration.) For example, in the CF₄/Ar and Cl₂/Ar measurements the axial distribution of metastables becomes more uniform at higher additive concentrations and lower powers, respectively, because of a relative enhancement of metastable density near the ground sheath/bulk interface. These observed changes in the metastable distribution largely result from changes in the spatially dependent metastable excitation rather than the destruction rate. This can be inferred by the similarity of the centerline ($r=0$), line-of-sight-averaged excited-state argon emission profiles (Fig. 7), which reflect only the production rate (see, e.g., Ref. 3), to the corresponding metastable profiles (Fig. 3), which reflect the balance between the spatially dependent production and destruction rates.

We attribute these spatial changes in the excited-state emission profiles in the CF₄/Ar and Cl₂/Ar discharges, in part, to the reduced electron number density and a discharge transition from electropositive toward electronegative character. Indeed, experiments with a much larger attaching gas concentration (e.g., 25% CF₄), which should ensure a predominantly electronegative character, showed similar changes in the emission profiles. The reduction in electron number density in the Cl₂/Ar and CF₄/Ar discharges occurs because of electron attachment reactions such as:²⁹



Based on a comparison of the electron attachment cross sections (see Refs. 28 and 29), one might expect the O₂/Ar discharges to exhibit a similar (electronegative) behavior to that observed for CF₄/Ar, because O₂ and CF₄ have similar cross sections. However, this was not observed in the present study. The O₂/Ar discharges examined here (all at 33.3 Pa, 200 V, and <4% O₂) were found to be essentially electropositive in nature, based on the similarity of the pure argon and O₂/Ar optical emission profiles. Presumably, the electropositive nature of these O₂/Ar discharges is due to a complex competition between various electron–impact dissociation and attachment, associative attachment, and ion–ion recombination reactions within the discharge, including, for example,





which leads to only a modest reduction in the electron number density at these conditions.

Although the complete reaction set necessary to describe the O_2/Ar discharge chemistry is obviously far more complex than this, a simple comparison of the rates for the former three reactions illustrates this competition. Assuming a Maxwellian distribution with an average electron energy of ~ 4 eV, for example, the rate coefficient for reaction (9) is more than an order of magnitude larger than that of Eq. (10), 1×10^{-9} compared to 3×10^{-11} cm^3/s .¹² Hence, neutral dissociation is favored and thus reduces potential electron losses (and the formation of O^-) through attachment. In addition, the rate coefficient for Eq. (11) is relatively large ($\sim 3 \times 10^{-10}$ cm^3/s);¹² consequently, associative attachment can act to replenish the electron number density at the expense of negative oxygen ions, thereby making the discharge more electropositive in nature. In a 1% O_2/Ar discharge at 33.3 Pa with 10% dissociation, for example, the rates for Eqs. (10) and (11) are comparable and on the order of 10^{12} $\text{cm}^{-3} \text{s}^{-1}$, based on estimated electron, O_2 , O, and O^- number densities of 10^9 , 10^{14} , 10^{13} , and 10^9 cm^{-3} , respectively.

It should be noted, though, that while the O_2/Ar discharges examined here were essentially electropositive, one might expect that some O_2/Ar discharges would show a more electronegative nature, perhaps at lower power or at higher oxygen concentrations. Recent modeling results by Sommerer and Kushner,³⁰ for example, show that pure oxygen rf discharges at similar conditions (33.3 Pa, 200 V) are electronegative in nature, with a relatively large negative ion density and substantially reduced electron density.

V. SUMMARY AND CONCLUDING REMARKS

In this experimental study, we examined the effect of minor (<5%) additions of attaching gases on the relative density and spatial distribution of the argon metastables in low-pressure, parallel-plate, rf argon plasmas. The diagnostics applied to the discharge included planar laser-induced fluorescence imaging to map the 2D metastable density distribution; optical emission measurements of excited-state argon to profile the metastable formation rate; and rf electrical measurements of voltage and current to determine the power deposition.

The addition of only a few percent of O_2 , Cl_2 , or CF_4 was found to decrease the metastable density by as much as an order of magnitude, despite the fact that the emission indicated an increase in the metastable production rate. This net decrease in metastable density was attributed to quenching by the respective molecular additives and their dissociation products. The largest decrease in metastable density was observed for Cl_2 , followed by O_2 , and CF_4 , which is consistent with the molecular quenching rates available in the literature.

The addition of Cl_2 and CF_4 was also found to significantly affect the spatial distribution of the emission intensity and metastable density as well, indicating a transition from an electropositive to an electronegative discharge. In the pure

argon (electropositive) and O_2/Ar discharges, the axial metastable density was strongly peaked near the powered sheath/plasma bulk interface, whereas, particularly at lower powers and/or higher attaching gas concentrations, the Cl_2/Ar and CF_4/Ar discharges showed a more uniform axial metastable profile. Given that these metastable measurements were obtained in a well-characterized reactor and that rather substantial changes in both the metastable densities and spatial distributions were observed, these data should provide a stringent test for future model validations.

ACKNOWLEDGMENTS

The authors would like to thank M. A. Sobolewski and J. R. Whetstone for their help with the plasma electrical measurements, and M. J. Kushner and D. J. Economou for helpful discussions regarding this work.

- ¹ *Computational Modeling in Semiconductor Processing*, edited by M. Meyyappan (Artech House, Boston, 1995).
- ² D. B. Graves, *IEEE Trans. Plasma Sci.* **22**, 31 (1994).
- ³ B. K. McMillin and M. R. Zachariah, *J. Appl. Phys.* **77**, 5538 (1995).
- ⁴ L. G. Piper, J. E. Velazco, and D. W. Setzer, *J. Chem. Phys.* **59**, 3323 (1973).
- ⁵ C. R. Aita and M. E. Marhic, *J. Appl. Phys.* **52**, 6584 (1981).
- ⁶ J. Balamuta, M. F. Golde, and A. M. Moyle, *J. Chem. Phys.* **82**, 3169 (1985).
- ⁷ G. R. Scheller, R. A. Gottscho, D. B. Graves, and T. Intrator, *J. Appl. Phys.* **64**, 598 (1988).
- ⁸ G. R. Scheller, R. A. Gottscho, T. Intrator, and D. B. Graves, *J. Appl. Phys.* **64**, 4384 (1988).
- ⁹ A. J. Paranjpe, J. M. McVittie, and S. A. Self, *J. Vac. Sci. Technol. A* **8**, 1654 (1990).
- ¹⁰ P. Bletzinger, *J. Appl. Phys.* **67**, 130 (1990).
- ¹¹ P. J. Hargis, Jr., K. E. Greenberg, P. A. Miller, J. B. Gerardo, J. R. Torczynski, M. E. Riley, G. A. Hebner, J. R. Roberts, J. K. Olthoff, J. R. Whetstone, R. J. Van Brunt, M. A. Sobolewski, H. M. Anderson, M. P. Splichal, J. L. Mock, P. Bletzinger, A. Garscadden, R. A. Gottscho, G. Seslwyn, M. Dalvie, J. E. Heidenreich, J. W. Butterbaugh, M. L. Brake, M. L. Passow, J. Pender, A. Lujan, M. E. Elta, D. B. Graves, H. H. Sawin, M. J. Kushner, J. T. Verdeyen, R. Horwath, and T. R. Turner, *Rev. Sci. Instrum.* **65**, 140 (1994).
- ¹² M. A. Lieberman and A. J. Lichtenberg, *Principles of Plasma Discharges and Material Processing* (Wiley, New York, 1994).
- ¹³ K. R. Ryan and I. C. Plumb, *Plasma Chem. Plasma Processing* **6**, 231 (1986).
- ¹⁴ N. L. Bassett and D. J. Economou, *J. Appl. Phys.* **75**, 1931 (1994).
- ¹⁵ *Plasma Etching: An Introduction*, edited by D. M. Manos and D. L. Flamm (Academic, Boston, 1989).
- ¹⁶ M. A. Sobolewski, *J. Vac. Sci. Technol. A* **10**, 3550 (1992).
- ¹⁷ M. A. Sobolewski, *IEEE Trans. Plasma Science* (submitted).
- ¹⁸ B. L. Preppernau and T. A. Miller, in *Glow Discharge Spectroscopies*, edited by R. K. Marcus (Plenum, New York, 1993).
- ¹⁹ R. K. Hanson, J. M. Seitzman, and P. H. Paul, *Appl. Phys. B* **50**, 441 (1990).
- ²⁰ L. J. Overzet and M. B. Hopkins, *Appl. Phys. Lett.* **63**, 2484 (1993).
- ²¹ G. S. Oehrlein and H. L. Williams, *J. Appl. Phys.* **62**, 662 (1987).
- ²² C. M. Ferreira and J. Loureiro, *J. Phys. D: Appl. Phys.* **16**, 1611 (1983).
- ²³ D. P. Lymberopoulos and D. J. Economou, *J. Appl. Phys.* **73**, 3668 (1993).
- ²⁴ L. Sansonnens, A. A. Howling, Ch. Hollenstein, J.-L. Dorian, and U. Kroll, *J. Phys. D: Appl. Phys.* **27**, 1406 (1994).
- ²⁵ A. P. Paranjpe, J. P. McVittie, and S. A. Self, *Phys. Rev. A* **41**, 6949 (1990).
- ²⁶ E. Gogolides and H. H. Sawin, *J. Appl. Phys.* **72**, 3971 (1992).
- ²⁷ M. A. Sobolewski and B. K. McMillin, National Institute of Standards and Technology, Gaithersburg, MD (unpublished).
- ²⁸ *Electron-Molecule Interactions and Their Applications*, edited by L. G. Christophorou (Academic, New York, 1984), Vol. 1.
- ²⁹ S. R. Hunter, J. G. Carter, and L. G. Christophorou, *J. Appl. Phys.* **58**, 3001 (1985).
- ³⁰ T. J. Sommerer and M. J. Kushner, *J. Appl. Phys.* **71**, 1654 (1992).